



Are Active Galactic Nuclei in Post-starburst Galaxies Driving the Change or Along for the Ride?

Lauranne Lanz¹, Sofia Stepanoff¹, Ryan C. Hickox², Katherine Alatalo^{3,4}, K. Decker French^{5,6}, Kate Rowlands^{4,7}, Kristina Nyland⁸, Philip N. Appleton⁹, Mark Lacy¹⁰, Anne Medling^{11,12}, John S. Mulchaey¹³, Elizaveta Sazonova⁴, and Claudia Megan Urry^{14,15}

¹ Department of Physics, The College of New Jersey, 2000 Pennington Road, Ewing, NJ 08628, USA

² Department of Physics and Astronomy, Dartmouth College, 6127 Wilder Laboratory, Hanover, NH 03755, USA

³ Space Telescope Science Institute, 3700 San Martin Dr, Baltimore, MD 21218, USA

⁴ Johns Hopkins University, Department of Physics and Astronomy, Baltimore, MD 21218, USA

⁵ Department of Astronomy, University of Illinois Urbana-Champaign, Urbana, IL 61801, USA

⁶ Center for Astrophysical Surveys, National Center for Supercomputing Applications, 1205 W. Clark St., Urbana, IL 61801, USA

⁷ AURA for ESA, Space Telescope Science Institute, 3700 San Martin Dr, Baltimore, MD 21218, USA

⁸ U.S. Naval Research Laboratory, 4555 Overlook Ave. SW, Washington, DC 20375, USA

⁹ IPAC, Mail Code 314-6, Caltech, 1200 E. California Blvd., Pasadena, CA 91125, USA

¹⁰ National Radio Astronomy Observatory, 520 Edgemont Road, Charlottesville, VA 22903, USA

¹¹ Ritter Astrophysical Research Center, University of Toledo, Toledo, OH 43606, USA

¹² ARC Centre of Excellence for All Sky Astrophysics in 3 Dimensions (ASTRO 3D)

¹³ The Observatories of the Carnegie Institution for Science, Pasadena, CA 91101, USA

¹⁴ Yale Center for Astronomy & Astrophysics, 46 Hillhouse Avenue, New Haven, CT 06511, USA

¹⁵ Department of Physics, Yale University, P.O. Box 208120, New Haven, CT 06520-8120, USA

Received 2021 August 25; revised 2022 June 20; accepted 2022 June 28; published 2022 August 10

Abstract

We present an analysis of 10 ks snapshot Chandra observations of 12 shocked post-starburst galaxies, which provide a window into the unresolved question of active galactic nuclei (AGN) activity in post-starburst galaxies and its role in the transition of galaxies from active star formation to quiescence. While seven of the 12 galaxies have statistically significant detections (with two more marginal detections), the brightest only obtained 10 photons. Given the wide variety of hardness ratios in this sample, we chose to pursue a forward-modeling approach to constrain the intrinsic luminosity and obscuration of these galaxies, rather than stacking. We constrain the intrinsic luminosity of obscured power laws based on the total number of counts and spectral shape, itself mostly set by the obscuration, with hardness ratios consistent with the data. We also tested thermal models. While all the galaxies have power-law models consistent with their observations, a third of the galaxies are better fit as an obscured power law and another third are better fit as thermal emission. If these post-starburst galaxies, early in their transition, contain AGNs, then these are mostly confined to lower obscuration ($N_H \leq 10^{23} \text{ cm}^{-2}$) and lower luminosity ($L_{2-10 \text{ keV}} \leq 10^{42} \text{ erg s}^{-1}$). Two galaxies, however, are clearly best fit as significantly obscured AGNs. At least half of this sample shows evidence of at least low-luminosity AGN activity, though none could radiatively drive out the remaining molecular gas reservoirs. Therefore, these AGNs are more likely along for the ride, having been fed gas by the same processes driving the transition.

Unified Astronomy Thesaurus concepts: Post-starburst galaxies (2176); Active galactic nuclei (16); Low-luminosity active galactic nuclei (2033); Galaxy evolution (594); X-ray astronomy (1810)

1. Introduction

Galaxies in the local universe show correlated bimodal distributions in color, star formation activity, and morphology, with the majority falling into either a blue actively star-forming spiral category or a red quiescent lenticular or elliptical category (e.g., Strateva et al. 2001; Baldry et al. 2004). The relative rarity of galaxies with intermediate colors, the “green-valley” galaxies, suggests a relatively rapid transition (Bell et al. 2003). However, green-valley galaxies, if selected based just on color, contain a mix of two populations: a smaller, rapidly quenched post-starburst population and a much larger, slower-quenching population, whose optical colors shift with the buildup of an older stellar population and the exhaustion of

their molecular gas (e.g., Noeske et al. 2007; Schawinski et al. 2014).

Selecting these rapid quenchers during their transition therefore requires spectral criteria, yielding populations called “E+A” or “K+A” galaxies (e.g., Zabludoff et al. 1996; Quintero et al. 2004; Goto 2007). This methodology selects for recent star formation activity on the basis of the H δ absorption associated with A stars, while excluding galaxies showing ionized emission lines that are associated with active star formation. This exclusion inevitably also removes galaxies with other energetic processes that could be involved in the quenching process, such as emission from active galactic nuclei (AGNs). Several new selection criteria have since emerged that are not as strict in excluding ionized emission (e.g., Wild et al. 2007; Yesuf et al. 2014; Alatalo et al. 2016a). The galaxies used in this study were selected via the Alatalo et al. (2016a) methodology and belong to a population referred to as shocked post-starburst galaxies (SPOGs). The SPOG selection retains galaxies with ionized emission that is consistent with shocks,

AGNs, and low-ionization nuclear emission regions (LINERs; Kauffmann et al. 2003; Kewley et al. 2006), but excludes those that fall within the star-forming region of the three-line diagnostic diagrams (Baldwin et al. 1981; Veilleux & Osterbrock 1987). The SPOG selection typically selects galaxies earlier in their transition than the classical E+A criteria, as discussed further below. As such, they likely contain more readily observable clues as to the process driving the transition to quiescence.

The SPOG sample was initially presented by Alatalo et al. (2016a), where the sample selection methodology was discussed in detail. This sample was also compared to the sample of classical post-starburst galaxies collected by Goto (2007), particularly in the color–magnitude space, demonstrating that SPOGs are generally bluer than the Goto post-starburst galaxies. As such, the inclusion of a larger range of gas emission-line ratios, as compared to emission-line cuts, tends to select galaxies that have on average younger stellar populations and are therefore earlier in their transition than classically selected post-starburst galaxies. Similarly, Ardila et al. (2018) found that SPOGs have bluer far-UV–near-UV colors than other post-starburst samples.

In French et al. (2018), the star formation histories of SPOGs were determined together with those of post-starburst galaxies, which were selected using cuts on $H\delta$ absorption and the absence of $H\alpha$ emission. In this study, UV and optical photometry, together with optical spectroscopy, were fit with stellar population models to obtain the star formation histories. Both sets of post-starburst galaxies showed similar histories and stellar mass distributions consistent with other post-starburst samples (e.g., Melnick & De Propriis 2013), but the SPOGs generally had younger ages, consistent with being recent progenitors of the comparison post-starburst samples. This result is in agreement with the blue optical and UV colors found by Alatalo et al. (2016a) and Ardila et al. (2018).

A major open question in galaxy evolution and, in particular, the transition from star formation to quiescence, is the role of AGNs in this process. Mergers have long been posited as a pathway for this transition (e.g., Toomre & Toomre 1972; Hopkins et al. 2006), and are effective at creating both periods of AGN activity (e.g., Springel et al. 2005a; Hopkins & Quataert 2010) and post-starburst galaxies in simulations (Lotz et al. 2021; Zheng et al. 2020). AGN feedback has also been shown to be effective as a means of quenching star formation in simulations (e.g., Springel et al. 2005b; Somerville et al. 2008), including in field post-starburst galaxies, specifically (Lotz et al. 2021). AGNs are also known to drive multiphase outflows that have the potential to strip their galaxies of star-forming gas (e.g., Sturm et al. 2011; Cicone et al. 2014) and inject shocks and turbulence into their host’s interstellar media (ISM; e.g., Alatalo et al. 2015; Lanz et al. 2016; Smercina et al. 2018), thereby reducing the star formation activity. As such, AGN feedback provides a viable means of explaining the quenching in post-starburst galaxies or the lack of resumption of star formation in the remaining molecular gas (French et al. 2015; Rowlands et al. 2015; Alatalo et al. 2016b).

However, the observational support for both of these ingredients, mergers and AGN feedback, in post-starburst galaxies is mixed. Depending on the study, the merger fractions in these galaxies can range from 15% to 70% (Zabludoff et al. 1996; Goto 2005; Yang et al. 2008; Pawlik et al. 2016; Sazonova et al. 2021). The lower end of this range is likely an

underestimate, due to fading signatures of mergers over time. However, alternative processes may also play a factor, particularly for galaxies in denser environments.

Similarly, observational evidence for the presence and activity of AGNs in post-starburst galaxies remains unclear, with a variety of results. Brown et al. (2009) found that roughly half of 24 K+A galaxies in the NOAO Deep Wide-Field Survey showed optical signatures consistent with AGNs or LINERs, and a third of the optically brighter galaxies had X-ray luminosities of $\sim 10^{42}$ erg s $^{-1}$, indicating a relatively high presence of AGN activity, if at a lower activity level. The sample selection was also explicitly biased against emission-line galaxies, thereby excluding AGNs and potentially underestimating the AGN fraction. The presence of AGNs in post-starburst galaxies is further supported by the stacking study undertaken by Georgakakis et al. (2008), which found evidence of a significant population of obscured AGNs in these galaxies. Yesuf et al. (2014) also found that 36% of quenching post-starburst galaxies showed optical signatures of AGNs, albeit delayed relative to the starburst peak, indicating that AGNs were likely not the cause of the quenching in most of these systems. De Propriis & Melnick (2014) showed that their sample of 10 K+A galaxies in a range of merger states lacked evidence of powerful AGNs, using both optical and X-ray indicators, but a large fraction of their sample had weak ($L_X \leq 10^{40}$ erg s $^{-1}$) X-ray emission.

Surveys at radio and infrared (IR) wavelengths found less support for the presence of AGNs. Cross-identification with the Faint Images of the Radio Sky at Twenty centimeters (FIRST; Becker et al. 1995) survey has been done for two samples of E+A galaxies (Shin et al. 2011; Nielsen et al. 2012), but while some enhanced radio emission was detected, it could not be unambiguously identified as AGN activity. More recently, two surveys of the IR emission of E+A galaxies (Alatalo et al. 2017; Meusinger et al. 2017) found enhanced mid-IR (MIR) emission that was potentially suggestive of AGNs, but did not meet the WISE color criterion indicative of luminous AGNs (e.g., Stern et al. 2012). While Melnick & De Propriis (2013) found that the MIR emission could be explained by thermally pulsing asymptotic giant branch (TP-AGB) stars or obscured AGNs, Alatalo et al. (2017) showed that WISE [12]–[22] colors of the Goto post-starburst galaxies are more consistent with AGNs than TP-AGB stars. Alatalo et al. (2016b) also examined the WISE emission in a sample of SPOGs with measurements or limits on molecular masses. In comparison to the correlation between molecular mass and IR luminosity found in star-forming samples, effectively a reframing of the Kennicutt–Schmidt (e.g., Kennicutt 1998) relation of constant star formation efficiency, SPOGs showed an excess of IR emission for their molecular content, as would be expected if additional heating were due to an AGN. However, the relatively small excess compared to radio galaxy AGNs suggests a conclusion similar to those for the E+A studies, namely, that the IR properties indicate either that AGNs are not especially common or that they are generally of low luminosity or radiatively inefficient.

To make progress in determining whether AGNs play a significant role in the transition process, we need an unambiguous measure of AGN activity. Therefore, we obtained Chandra observations of a set of 12 SPOGs selected from the original sample of 1067 (see Alatalo et al. 2016a for a discussion of the SPOG selection criteria) that have a FIRST

Table 1

IAU Name (1)	SPOG Number (2)	CXO Name (3)	R.A. (hms) (4)	Decl. (dms) (5)	Redshift (6)	Dist. (Mpc) (7)	$F_{1.4}$ (mJy) (8)	MW nH (9)	ObsID (10)	Obs. Date (11)	Exposure Time (12)
J001145–005431	4	38	00:11:45.2	–00:54:30.6	0.0479	215	2.08	3.48	19480	2017-8-9	9.99
J085357+031034	157	10	08:53:56.8	+03:10:33.6	0.1292	613	1.25	3.16	19486	2017-1-11	9.91
J091407+375310	186	1562	09:14:07.2	+37:53:10.0	0.0719	328	2.60	1.50	19484	2017-1-11	9.93
J093820+181953	224	1070	09:38:19.9	+18:19:52.7	0.0886	409	4.52	2.57	19485	2017-3-8	9.93
J095750–001239	253	2178	09:57:49.5	–00:12:39.2	0.0330	146	0.86	2.77	19479	2017-3-30	9.91
J102653+434008	305	1558	10:26:53.4	+43:40:08.4	0.1053	492	1.30	1.20	19481	2018-3-3	9.92
J113655+245325	462	1030	11:36:55.2	+24:53:25.4	0.0327	145	2.55	1.93	19478	2017-2-2	10.80
J113939+463132	470	1557	11:39:39.3	+46:31:32.2	0.1735	847	4.95	1.97	19489/20829	2017-10-27	4.88/4.89
J115341+093026	498	5260	11:53:41.3	+09:30:25.6	0.1389	663	1.56	1.73	19483	2017-2-10	9.93
J131448+210626	662	1081	13:14:47.6	+21:06:26.3	0.0458	205	1.97	2.75	19487	2016-11-17	9.80
J132648+192246	689	1147	13:26:48.1	+19:22:45.7	0.1741	850	2.09	1.61	19488	2017-3-11	9.91
J155525+295551	955	2	15:55:24.9	+29:55:50.9	0.0699	319	2.96	2.83	19482	2016-12-14	9.82

Note. (1): IAU name. (2): ID number from Alatalo et al. (2016a, Table 2), which differs from the earlier numbering used at the time of the Chandra proposal (3), included here for ease of reference relative to the archive. (4) and (5): J2000 coordinates. (6): Sloan Digital Sky Survey spectroscopic redshift. (7): Distance in Mpc determined from the redshift, assuming the WMAP 9 cosmology (Hinshaw et al. 2013). (8): Integrated 1.4 GHz flux density from FIRST observations from Alatalo et al. (2016b, Table 2). (9): Foreground Milky Way column density (nH) in units of 10^{20} cm^{-2} (HI4PI Collaboration et al. 2016). (10): Chandra observation ID. (11): Observation date. (12): Exposure time in ks.

Table 2
Counts and Hardness Ratios

IAU Name (1)	SPOG Number (2)	(Net) Counts			Significance 0.5–8 keV (6)	Hardness Ratio (7)
		0.5–8 keV (3)	0.5–2 keV (4)	2–8 keV (5)		
J001145–005431	4	8 (7.7)	3 (2.9)	5 (4.8)	6.2	0.24 ([–0.07, 0.58])
J085357+031034	157	10 (9.7)	1 (0.9)	9 (8.8)	7.3	0.79 ([0.69, 1.00])
J091407+375310	186	3 (2.7)	1 (0.9)	2 (1.8)	2.9*	0.30 ([–0.01, 1.00])
J093820+181953	224	3 (2.7)	2 (1.9)	1 (0.8)	2.9*	–0.40 ([–1.00, –0.12])
J095750–001239	253	6 (5.7)	5 (4.9)	1 (0.8)	4.8	–0.72 ([–1.00, –0.56])
J102653+434008	305	1 (0.7)	1 (0.9)	0 (0)	1.1 [†]	–0.64 ([–1.00, –0.27])
J113655+245325	462	5 (4.7)	4 (3.9)	1 (0.8)	4.3	–0.65 ([–1.00, –0.47])
J113939+463132	470	7 (6.7)	6 (5.9)	1 (0.8)	5.7	–0.74 ([–1.00, –0.60])
J115341+093026	498	4 (3.7)	2 (1.9)	2 (1.8)	3.6	–0.05 ([–0.53, 0.48])
J131448+210626	662	4 (3.7)	2 (1.9)	2 (1.8)	3.7	–0.05 ([–0.50, 0.49])
J132648+192246	689	2 (1.7)	1 (0.9)	1 (0.8)	2.1 [†]	–0.05 ([–1.00, 0.29])
J155525+295551	955	2 (1.8)	1 (0.9)	1 (0.8)	2.3 [†]	–0.09 ([–1.00, 0.24])

Note. (3)–(5): Total counts, with background-subtracted net counts in parentheses, in the total, soft, and hard bands. (6): Statistical significance of the total net count detection. See Section 2.1 for an explanation of their derivation. Marginal detections are marked with “*,” while non-significant detections are marked with “[†].” (7): Median hardness ratio, with the 1σ range given in parentheses from BEHR (Park et al. 2006).

counterpart, a detected $22 \mu\text{m}$ emission, and a CO detection with either CARMA or IRAM (Alatalo et al. 2016b). These galaxies were among the most likely SPOGs to contain an AGN, and the CO measurements allowed at least an initial estimate of the obscuration column. We present the results of this investigation here.

This paper is organized as follows. In Section 2, we describe the observations and their analysis. We explain the forward-modeling methodology that we used to constrain the AGN properties in Section 3. The results of this analysis are discussed in Section 4, and their implications are explained in Section 5. Finally, we summarize the paper in Section 6. We assume the Wilkinson Microwave Anisotropy Probe (WMAP) 9 cosmology, with $H_0 = 69.3 \text{ km s}^{-1} \text{ Mpc}^{-1}$, $\Omega_\Lambda = 0.713$, and $\Omega_M = 0.287$ (Hinshaw et al. 2013).

2. Observations and Data Analysis

Table 1 summarizes our observations (P.I.: L. Lanz). Each galaxy was observed for ~ 10 ks between 2016 November 17 and 2018 March 3, mostly in a single observation. Each of the galaxies were centered on the aimpoint of the back-illuminated S3 chip of the Chandra Advanced CCD Imaging System (Weisskopf et al. 2000) in VFaint mode. We reprocessed the observations using CIAO version 4.13 to create new level 2 event files. We measured the counts in the total (0.5–8 keV), hard (2–8 keV), and soft (0.5–2 keV) bands, in $2''$ apertures centered on the galaxy, as well as a larger background region within the S3 chip. For SPOG470, we measured the counts on each event file and combined them to get the counts obtained over the full ~ 10 ks. Table 2 lists the results, and Figure 1 shows the aperture placed on each total image.

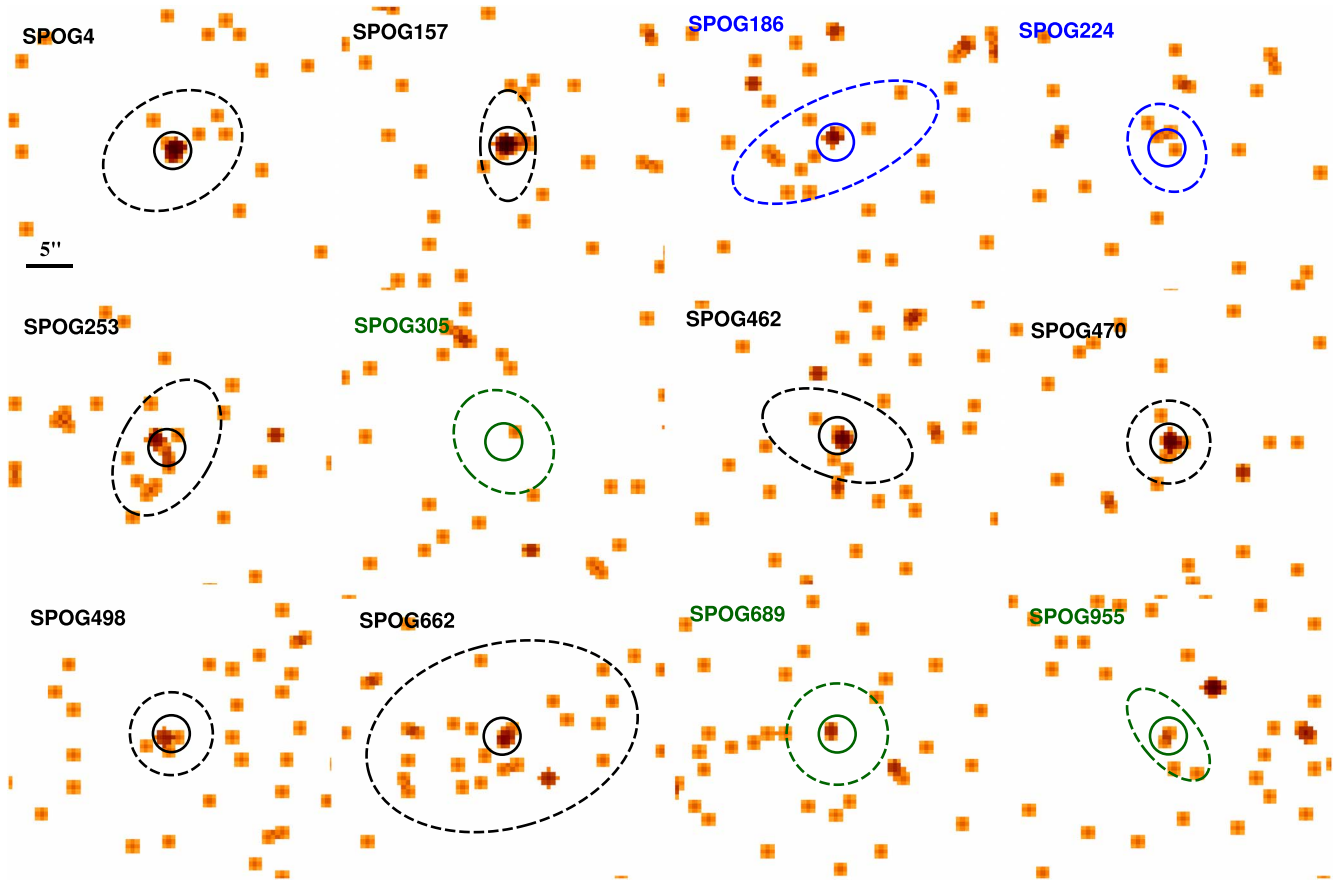


Figure 1. Images of the 0.5–8 keV emissions of the 12 SPOGs, with the 2'' aperture overlaid. The dashed ellipses are the approximate extents of the Sloan Digital Sky Survey r emissions, denoting the sizes of the galaxies. The colors of the labels and regions indicate whether the detection is significant (black), marginal (blue), or non-significant (green). Slight Gaussian smoothing is applied to help highlight the presence of the source.

2.1. Determination of Statistical Significance

Since we are clearly in the realm of small-number statistics, we use Poisson statistics to determine the probability of getting the observed number of counts, given the background level (Gehrels 1986). The Poisson probability of getting fewer than or equal to x events, given an expected rate of b set by the background estimated for the aperture, is

$$P(x, b) = \sum_{k=0}^x e^{-b} \frac{b^k}{k!}. \quad (1)$$

To determine the probability of the photons in the aperture being background emission, what we need is the probability of getting at least x events, which is therefore given by

$$P_2(x, b) = 1 - \sum_{k=0}^{x-1} e^{-b} \frac{b^k}{k!}, \quad (2)$$

since detections of photons are discrete events. The typical estimated background level in the source aperture is ~ 0.3 counts in the 0.5–8 keV band, of which ~ 0.1 come from the 0.5–2 keV band and the other ~ 0.2 come from the 2–8 keV band. For simplicity of interpretation, we then convert these probabilities to Gaussian σ values using

$$P_2(x, b) = \text{erf}\left(\frac{\sigma}{\sqrt{2}}\right). \quad (3)$$

Probabilities consistent with $\sigma \geq 3$ are considered statistically significant. Those with probabilities less than 1% of being background fluctuations, corresponding to $\sigma \gtrsim 2.6$, are considered marginal detections. The σ values for the full 0.5–8 keV band are reported in Table 2.

2.2. Hardness Ratio Determination

Due to the low photons counts, we chose to use the Bayesian Estimation of Hardness Ratios (BEHR; Park et al. 2006) to determine the likely range of hardness ratios consistent with our data. Hardness ratios provide a sense of the spectral shape, particularly in the absence of sufficient counts for spectral fitting. We use 0.5–2 keV as our soft band (S) and 2–8 keV as the hard band (H), with the hardness ratio defined as

$$\text{HR} = \frac{H - S}{H + S}. \quad (4)$$

BEHR takes the total source counts in each band, as well as the total background counts in each band, and a ratio of the background aperture area to the source aperture area. A Bayesian approach coupled with Monte Carlo sampling is used to determine the posterior distribution for the hardness ratio. In Table 2, we report the median of that distribution, in addition to the 1σ range.

2.3. Why Not Stack?

A common approach when faced with a sample of similar objects with few counts is to stack the spectra and fit the resulting spectrum to get an average sense of the X-ray properties of these objects. Although these are all post-starburst galaxies, we decided that this route would provide limited useful information, for two main reasons. First, even including the marginal detections and nondetections, we only had a total of 55 counts, of which approximately 1.2 are from the background (with only the significant detections, we only have 44 counts). This stacked spectrum would therefore provide very poor constraints on any obscuration, as well as on the slope of the intrinsic power law.

Second, and more importantly, while the X-ray emission is indeed measured from the centers of the galaxies, it is unclear whether this is always due to power-law AGN emission in these sources. This concern emanates from the much deeper 150 ks Chandra observation undertaken on the local post-starburst galaxy NGC 1266¹⁶ (Alatalo et al. 2015; L. Lanz et al. 2022, in preparation). The majority of NGC 1266’s X-ray emission, while concentrated within a few arcseconds of the AGN, is clearly extended, soft, best modeled as a thermal plasma, and coincident with a multiphase outflow. Its AGN appears to be both highly obscured and relatively low in luminosity. As such, NGC 1266 is a clear example of a post-starburst galaxy whose X-ray emission is not dominated by power-law emission. Additionally, radio galaxies, including local early-type galaxies, have been shown to have significant thermal X-ray emission, due to the shocks driven by their jets, as also traced by warm molecular hydrogen emission (Lanz et al. 2015). Since the SPOG selection specifically allows galaxies with emission-line ratios consistent with shocks, some of the selected galaxies may have X-ray emission more consistent with thermal emission than power-law emission.

While the hardness ratios of this sample are not tightly constrained, their median values have a large range, from the very soft, at -0.72 (SPOG253), to the very hard, at 0.79 (SPOG157). Further, they approximately divide into thirds as hard, soft, or intermediate-hardness sources. This suggests either a mix of power-law-dominated and thermal-dominated systems and/or a variety of obscuration levels, from minimal to high. Therefore, stacking such a heterogenous group would not provide reliable constraints.

3. Forward-modeling Methodology

To obtain constraints on the nuclear properties of these galaxies, we therefore turned to forward modeling. We have two main constraints: the number of counts observed and their hardness ratios. The first effectively constrains the normalization of any model, as a brighter object will yield more counts in a given exposure time. The second provides a proxy of spectral shape. To generate mock spectra for each galaxy, we needed the Chandra response files (rmf and arf) at the time of the observation, as well as the exposure time. We used *sherpa* (Freeman et al. 2001; Doe et al. 2007) to extract

¹⁶ NGC1266 is a specifically interesting comparison for SPOGs, because it has optical emission-line characteristics that would have been selected against when using classical post-starburst selection criteria, but not when using the SPOG selection criteria (Alatalo et al. 2016a).

response files from each observation,¹⁷ so that the simulated spectra would be consistent with the specific response at the time of the observation of each galaxy.

For each galaxy, we tested two model types: an absorbed power law, to represent a classical AGN-dominated system, and a thermal plasma, as an alternative, to represent systems in which outflows or shocked emission dominates. We limit this analysis to these two simple models in order to avoid overfitting the limited constraints that we have, as discussed in the previous paragraph. With effectively two data points per galaxy, our models can have two free parameters, at most. This pair of model types spans the range of potential AGN-driven X-ray emission, and a recent study of nearby galaxies (Williams et al. 2022) showed that obscured power laws with or without a thermal component worked well for a large range of AGN luminosities, including Seyfert galaxies and LINERs.

For the power-law model, these free parameters are the local obscuration (N_H), applied with an *xsphabs* photoelectric absorption model, and an intrinsic 2–10 keV luminosity, used to determine the normalization of the power law in combination with the distance to the galaxy. The photon index is fixed to 1.8 (Piconcelli et al. 2005; Dadina 2008). We tested 416 different models, consisting of 16 values of local obscuration between 10^{21} and 10^{24} cm⁻², in steps of $10^{0.2}$, and 26 intrinsic luminosities between 10^{39} and 10^{44} erg s⁻¹, also in increments of $10^{0.2}$.

The free parameters of the thermal model are the plasma temperature (kT) of an *APEC* (Smith et al. 2001) model and an intrinsic 0.5–8 keV luminosity, which sets the normalization of the model. We also tested 416 different models, consisting of 16 temperatures between 0.5 and 2 keV, in steps of 0.1, and 26 intrinsic luminosities between 10^{37} and 10^{42} erg s⁻¹, in increments of $10^{0.2}$. For both models, we also applied an additional *xsphabs* to account for foreground Galactic absorption (Table 1, column 8).

For each model, we start by generating a spectrum with a long exposure time of unobscured emission, and we use the flux of the specific model to determine the normalization of the power law or *APEC* model such that it would yield the expected flux. We then create a new model by including the obscuration component(s), as appropriate, and generate 1000 separate spectra for the exposure taken of the specific galaxy (Table 1, column 11). We used *sherpa* to generate all of these mock spectra. For each spectrum, we calculate the counts in the 0.5–8 keV, 0.5–2 keV, and 2–8 keV bands, which are saved to a file per model. This process is repeated for each of the 832 models per galaxy, and for each galaxy.

We then analyzed these data to generate five maps of the model parameter space. First, we determine the average number of counts and the average hardness ratio in the simulated spectra for each model (Figures 2(a)–(b) and 3(a)–(b)). The average hardness ratio is determined by calculating the hardness ratio for each spectrum and then averaging the results. These two maps are primarily sanity checks. As expected, low-obscuration, high-luminosity (the lower right of Figure 2a) models of the power law show high numbers of counts, while high-obscuration, low-luminosity (upper left) show few counts. For thermal models, in contrast, the number of counts (Figure 3(a)) depends almost entirely on the

¹⁷ Since the two observations of SPOG470 were taken on the same day, we used the response from the first observation, as the difference between the response files would be minimal.

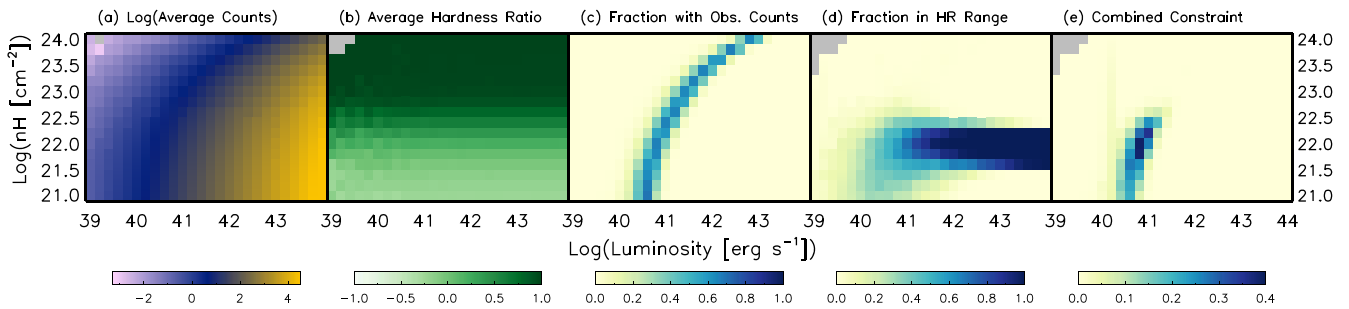


Figure 2. Example of the analysis of a set of power-law models, in this case for SPOG4. The X-axis has the intrinsic 2–10 keV luminosity of the AGN, while the Y-axis has the local obscuration column. (a) The average number of counts in the 0.5–8 keV band for each model, colored with a log scale. Low-obscuration, high-luminosity models yield the most counts. (b) The average hardness ratio of the spectra for each model. Higher-obscuration models have harder spectra. (c) The weighted fraction of the spectra for each model with counts consistent with the observed number for SPOG4 (see Section 3 for details). As is to be expected, more luminous models are necessary to get a certain photon flux when the obscuration is higher. (d) The fraction of the spectra for each model with hardness ratios within the range given in Table 2 (column 7). More luminous models yield more counts and therefore less scatter in their associated hardness ratios. (e) The fraction of the spectra per model meeting both the photon flux (c) and hardness ratio (d) constraints. The gray squares indicate models where less than five spectra of the 1000 have nonzero counts, meaning that the model does not really have a good measure of its hardness ratio.

luminosity, since the foreground Milky Way obscuration is minor. The hardness ratio plots (Figures 2(b) and 3(b)) show that, as expected, this quantity broadly does not depend on luminosity, as hardness ratios probe spectral shape, which is primarily determined by the amount of obscuration or the plasma temperature. Hardness ratios tend to be soft for thermal models.

Second, we implement our normalization constraint and calculate what fraction of the spectra for each model yielded 0.5–8 keV counts in the range of the observed number for that galaxy (Table 2, column 3), plus or minus the Gehrels uncertainty (Gehrels 1986), weighted by the Poisson probability of observing that many counts if the observed number is the true value.¹⁸ This weighting favors models creating large numbers of spectra with the observed number of counts, while taking into account a plausible range consistent with that number, due to the uncertainty as to how well the observed photon flux represents the true photon flux, given the short finite observation duration, as well as the effect of the ~ 0.3 counts from the background. Examples are shown in Figures 2(c) and 3(c). However, the trends seen are independent of whether we apply this weighting or only count the spectra with the exact number observed.

Third, we undertake a similar calculation for the hardness ratio, determining the fraction of spectra for each model that have hardness ratios in the range measured with BEHR for the observation (Table 2, column 7; Figures 2(d), 3(d)). Here, we do not apply weighting, and instead count all the models within the BEHR range. The reason for doing so is that a large fraction of our galaxies only have one count in one of the bands. This is taken into account as part of the BEHR analysis, but, as also indicated by the large ranges, means that the median hardness ratios are relatively uncertain. Finally, we combine these two constraints to determine the likelihood that a particular model will yield spectra consistent with the flux and spectral shape of the observations (Figures 2(e), 3(e), 4, and 5).

¹⁸ As an example, SPOG4 has eight observed counts and we consider spectra with five to eleven counts as within the range consistent with that observation. However, while mock spectra with eight counts are fully counted, a spectrum with five counts would be assigned a 65.6% weight (the Poisson probability of getting five photons per observation from an expected rate of eight).

4. Results

Figures 4 and 5 show the results of the forward-modeling analysis for the power-law and APEC models, respectively. In comparing the results of these models, we see that the galaxies broadly fall into three groups. The first set show much better agreement with one model type or the other: SPOG4 and SPOG157 essentially cannot be reproduced with thermal models, while SPOG253 has much stronger agreement with a thermal model. The second set are not as strongly preferential for one model versus another, but have a clear distinction between the highest probability of a thermal versus a power-law model: SPOG224, SPOG462, and SPOG470 are reproduced more easily with thermal models, while SPOG186, SPOG498, and SPOG662 are more likely to originate from a power-law model. The distinction between these two sub-groups is also consistent with their relative hardness ratios (Table 2, column 7), as the first subset is distinctly softer than the second. Finally, we have the remaining three galaxies (SPOG305, SPOG689, and SPOG955), where the modeling primarily places some constraints on luminosity and obscuration, but does not particularly otherwise narrow the parameter space. These are the three SPOGs with non-significant (even marginal) detections, so it is not altogether surprising that the constraints are the weakest in their cases.

Table 3 lists the parameters of the model with the highest probability and the range of model parameters over which at least 5% of the simulated spectra are consistent with the observations (corresponding to the dotted line contours in Figure 6). For SPOG4, SPOG157, and SPOG253, where one model is clearly better than the other, we only include the parameters of that model. When one model type appears more likely than the other, we bold the name of the model type. As can be seen in right column (panel c) of Figure 4, the model parameters of the obscured power law consistent with the observations are correlated—i.e., a more obscured source must also be brighter to yield a similar number of counts.

To illustrate the correlated uncertainties on intrinsic luminosity and obscuration for the power-law models shown in Figures 4 and 5, we plot error ellipses in Figure 6 (left). The best match between the model and the observed constraint is shown with the filled square. Models outside the dotted line have less than a 5% likelihood of resulting in our observation, so they are rejected with 2σ confidence. The dashed and solid lines show similar constraints at 1.5σ and 1σ , respectively.

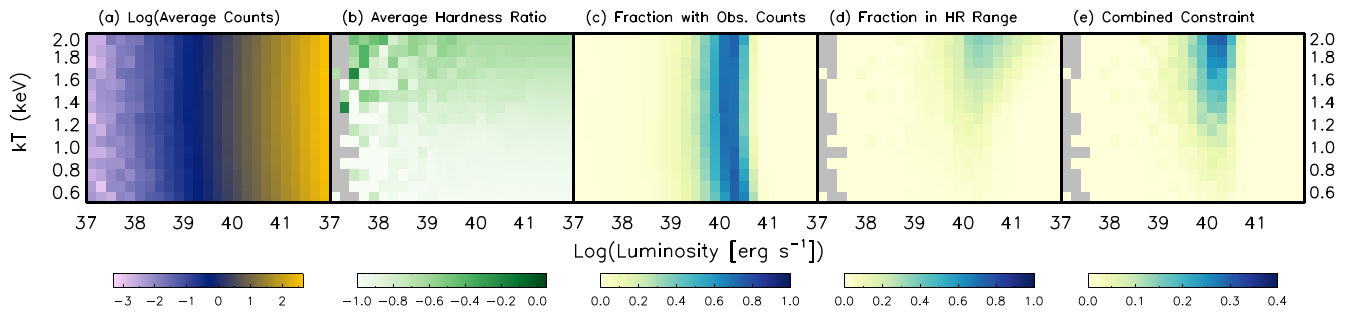


Figure 3. Example of the analysis of a set of thermal plasma models, in this case for SPOG662. The panels are broadly similar to those of Figure 2. However, here the X-axis is the 0.5–8 keV luminosity of the plasma, and the Y-axis is the temperature of the plasma. In thermal plasma models, the number of counts (a) does not depend much on the temperature for a given luminosity. However, the temperature sets the hardness ratio (b). Hotter plasmas have harder spectra, but all are generally soft. Since the hardness range from the Δ PEC models is narrower, it can provide a relatively strong constraint for galaxies with harder spectra but it is less effective as a constraint (d) for galaxies with softer emission. The photon flux constraints (c) tend to constrain the 0.5–8 keV luminosity within approximately an order of magnitude.

These show that higher-intrinsic luminosity models generally require more obscuration to be consistent with our observation, though this is most stringent for SPOG 157. Figure 6 (right) shows the equivalent figure for thermal models, demonstrating that while luminosity is generally constrained, temperature is not well constrained for these models.

4.1. Constraints on Average Nuclear Properties of the Sample

Taken together, these observations and analyses paint a relatively consistent picture regarding the AGN activity in SPOGs. While two plausible explanations could be given for the low photon flux, low luminosity or high obscuration, the forward-modeling analysis indicates that most of these galaxies appear to have moderate obscuration and relatively low luminosities, at most. The large majority of the sample have obscurations of $N_H \leq 10^{22} \text{ cm}^{-2}$ and intrinsic 2–10 keV luminosities of $L_X \leq 10^{42} \text{ erg s}^{-1}$. For the significantly detected sources, we can also put a lower limit on the likely luminosity of $L_X \geq 10^{40} \text{ erg s}^{-1}$, indicating that most of these AGNs would be Seyfert-like in their luminosities or low-luminosity AGNs.

4.1.1. The Exceptions: SPOG157 and SPOG186

Two SPOGs, SPOG157 and, to a lesser degree, SPOG186, show a different tendency. SPOG157 requires $N_H \geq 10^{23} \text{ cm}^{-2}$, particularly to explain its very hard spectrum. While the model with the highest fraction of mock spectra in agreement with the observed constraints has a parameter pair of $(L_X, N_H) = (3 \times 10^{43} \text{ erg s}^{-1}, 6 \times 10^{23} \text{ cm}^{-2})$, the six models in Figure 4(c) for SPOG157 with the darkest blue color have a similar fraction of mock spectra in agreement with the observations. They extend from $(L_X, N_H) = (3 \times 10^{42} \text{ erg s}^{-1}, 1 \times 10^{23} \text{ cm}^{-2})$ to $(L_X, N_H) = (6 \times 10^{43} \text{ erg s}^{-1}, 1 \times 10^{24} \text{ cm}^{-2})$, indicating that SPOG157 is more luminous and more obscured than most of the sample.

SPOG186 is only marginally detected, so its constraints are weaker. It too has a best-fit model with a higher obscuration, although not as high a luminosity, of $(L_X, N_H) = (4 \times 10^{41} \text{ erg s}^{-1}, 3 \times 10^{23} \text{ cm}^{-2})$. Its set of six models with similarly high fractions of mock spectra in agreement with the observed constraints has a parameter pair range extending from $(L_X, N_H) = (3 \times 10^{41} \text{ erg s}^{-1}, 2 \times 10^{23} \text{ cm}^{-2})$ to $(L_X, N_H) = (4 \times 10^{42} \text{ erg s}^{-1}, 1 \times 10^{24} \text{ cm}^{-2})$.

Given that the range of similarly well-fit models for both of these extends up to the $N_H = 1 \times 10^{24} \text{ cm}^{-2}$ limit of the model parameters, it is possible that one or both could have Compton-

thick obscuration. However, the absorption model used, XSPEC’s photoelectric absorption (phabs; xspfabs in sherpa), ceases to apply when the obscuration becomes optically thick at $N_H \gtrsim 1 \times 10^{24} \text{ cm}^{-2}$ (e.g., Maiolino & Risaliti 2007). Testing the parameters in this range would require a more complex model (e.g., BORUS; Baloković et al. 2018) that has more free parameters, thereby making them difficult to constrain with the limited data available for these galaxies.

5. Discussion

5.1. AGNs in Transitioning Galaxies

The overarching question that this study sought to help address was the role of AGNs in the transition of galaxies from active star formation to quiescence. The X-ray observations we have taken suggest that a large fraction ($\approx 58\%–75\%$) appear to have at least a moderate degree of nuclear activity. What is clear, though, is that we are not detecting bright obscured or unobscured quasars, as in the major-merger evolutionary scenario (e.g., Sanders et al. 1988; Hopkins et al. 2008; Alexander & Hickox 2012). As such, it is clear that these AGNs are not capable of radiatively driving out the star-forming fuel and driving the transition to quiescence. Rather, it seems that the mechanisms that started them on this transition are likely to have directed gas to the centers of these galaxies and thereby fed the accretion flow of these supermassive black holes.

Sazonova et al. (2021) recently undertook a morphological analysis of 26 SPOGs observed with the Hubble Space Telescope, finding that 27% show clear evidence of recent merger activity and another 30% show disturbances. Due to the fading of the merger signatures over time, it is difficult to conclude whether all the disturbances are the results of merger activity or whether alternative internal processes, such as AGN-driven outflows, may cause at least some of them.

Six galaxies were common between that subsample of SPOGs and those studied here. Interestingly, both SPOG157 and SPOG186 appear to be edge-on dusty disk galaxies, suggesting that at least some part of their obscuration may be on the galactic scale, rather than purely at the nuclear scale. The other four galaxies (SPOG4, SPOG224, SPOG253, and SPOG305) show disturbed but bulge-dominated morphologies without the tidal features that would indicate a clear tidal origin. On the X-ray front, these four galaxies span the range of hardness ratios (excluding SPOG157 and SPOG186) and are

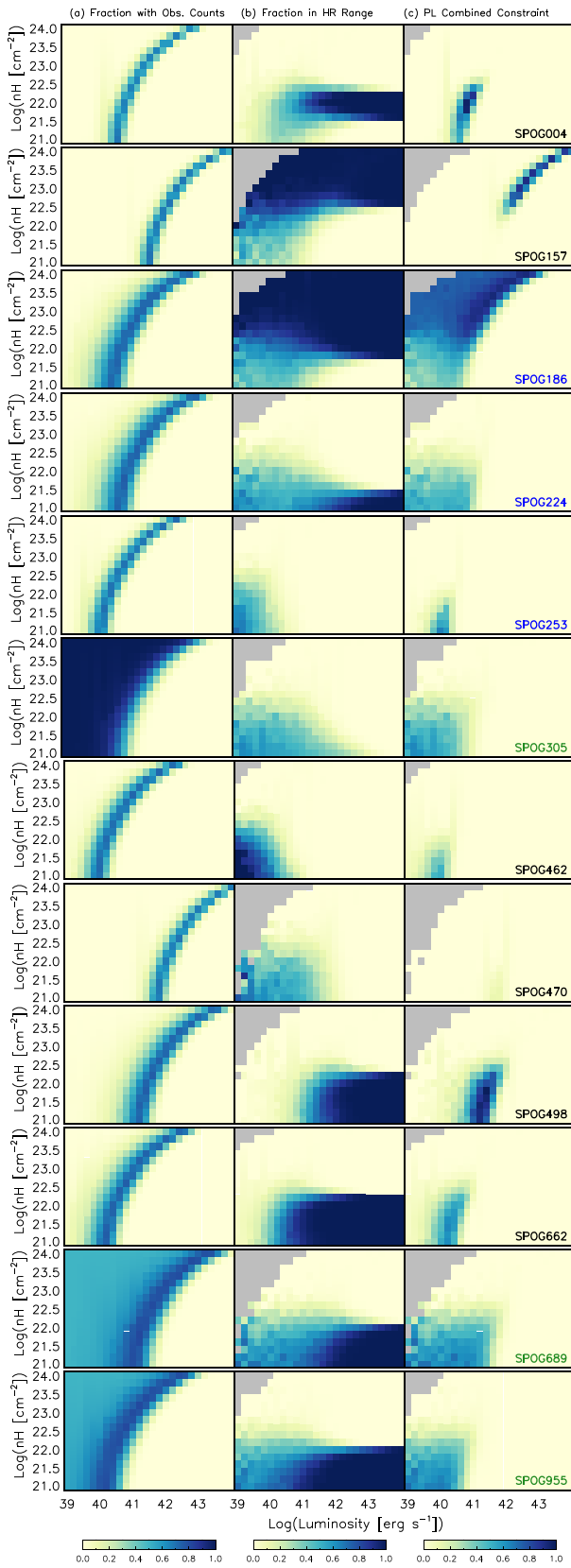


Figure 4. Results of the power-law model analysis for each SPOG, in numerical order. The left column shows the photon flux constraint, the middle column shows the hardness ratio constraint, and the right column shows the combined constraints. The gray squares are models with fewer than 0.5% of the spectra having nonzero counts. The color of the galaxy name has the same meaning as in Figure 1.

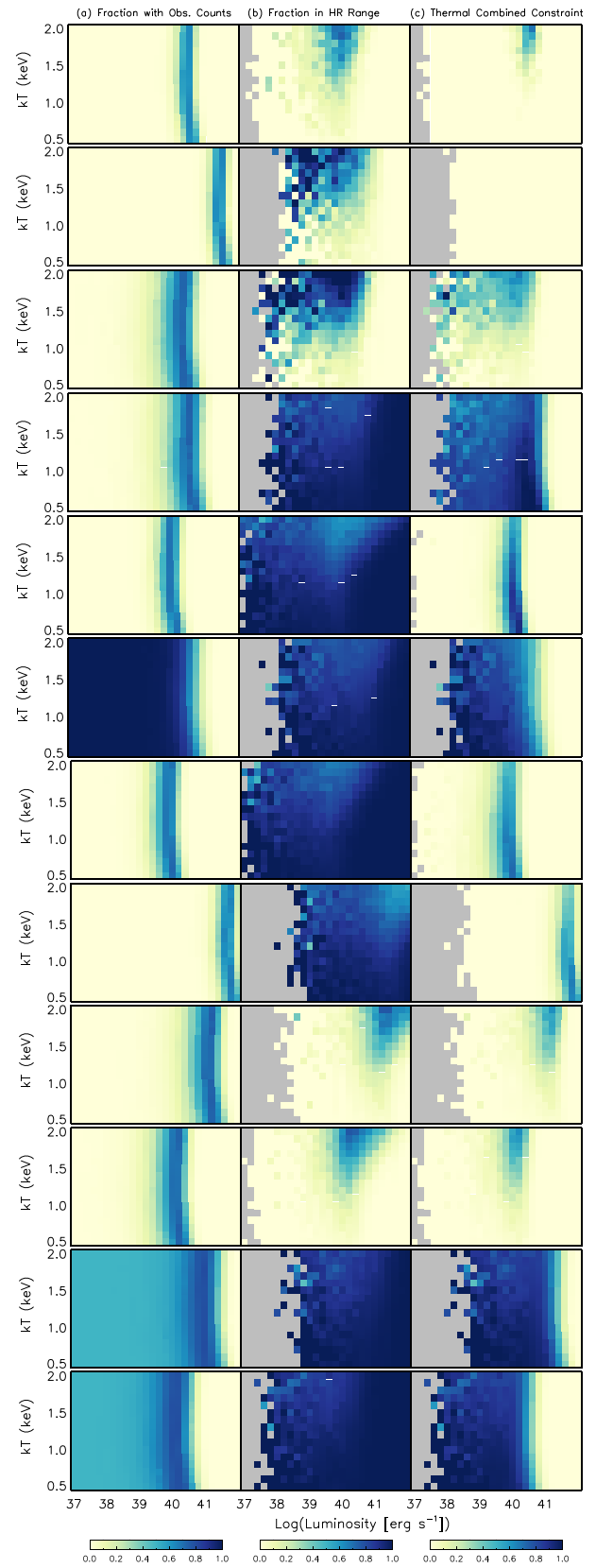


Figure 5. Results of the APEC model analysis for each SPOG in numerical order. The left column shows the photon flux constraint, the middle column shows the hardness ratio constraint, and the right column shows the combined constraints. The gray squares are models with fewer than 0.5% of the spectra having nonzero counts. For more distant galaxies, this corresponds to higher luminosities.

Table 3
Parameter Constraints

IAU Name (1)	SPOG Number (2)	Model Type (3)	Luminosity		Obscuration		Temperature		Notes (10)
			Best (4)	Range (5)	Best (6)	Range (7)	Best (8)	Range (9)	
Significantly Detected Galaxies									
J001145–005431	4	PL	40.8	40.4–41.2	22.0	≤22.6			(a)
J085357+031034	157	PL	43.4	41.8–44.0	23.8	22.2–24			(a)
J095750–001239	253	APEC	40.2	39.2–40.6			0.5	0.5–2.0	(b)
J113655+245325	462	PL	40.0	39.2–40.4	21.0	≤22.0			(d)
		APEC	40.0	37.4–40.4			0.6	0.5–2.0	
J113939+463132	470	PL	41.8	41.4–42.0	21.2	≤21.8			(d)
		APEC	41.8	41.2–42.0			0.7	0.5–2.0	
J115341+093026	498	PL	41.4	40.2–42.0	21.8	≤22.6			(c)
		APEC	41.2	38.6–41.6			2.0	0.8–2.0	
J131448+210626	662	PL	40.2	39.0–41.0	21.4	≤22.6			(c)
		APEC	40.2	39.2–40.4			2.0	0.8–2.0	
Marginally Detected or Non-significantly Detected Galaxies									
J091407+375310	186	PL	41.6	39.0–43.2	23.4	≤24			(c)
		APEC	38	37.4–40.6			1.7	0.6–2.0	
J093820+181953	224	PL	39.2	≤41.2	21.4	≤23.2			(d)
		APEC	40.6	37.6–41.2			0.6	0.5–2.0	
J102653+434008	305	PL	39.2	≤41.2	21.2	≤23.0			(e)
		APEC	≤40	≤41.2				0.5–2.0	
J132648+192246	689	PL	≤41.2	≤42	≤22	≤22.8			(e)
		APEC	≤41.4	≤41.8				0.5–2.0	
J155525+295551	955	PL	≤40.4	≤41.2	≤21.8	≤22.8			(e)
		APEC	≤40.2	≤41.0				0.5–2.0	

Note. (3) Model type: PL is the power-law model and APEC is the thermal model. (4) Luminosity of the model with the highest probability, if the models appear well constrained in Figures 4 and 5. (5) Range of luminosities over which there are models with at least 5% of the spectra being consistent with the observations. Models outside this range are rejected at the 95% level. Luminosities are 2–10 keV for power-law models and 0.5–8 keV for APEC models. (6–8) Similar constraints on the obscuration column and plasma temperature. (9) Notes on the relative merits of the two models: (a) the power-law model is much better; (b) the thermal model is much better; (c) the power-law model appears to be better; (d) the APEC model appears to be better; or (e) neither model is well constrained.

representative of the luminosity range and model types of the other six galaxies. As such, similar processes may be generating the X-ray emission in all these galaxies.

The presence of morphological disturbances indicates either the likely presence of mechanisms that could bring gas to the supermassive black holes, turning them into modest AGNs, or the effects of current or recent AGN mechanical feedback, driving an outflow or turbulence into the host galaxy and generating signatures of disturbances. In the former case, the active AGN would manifest as the power-law emission in X-rays (e.g., SPOG4 or SPOG498). In the latter case, AGN-driven outflows are often multiphase and can include hot X-ray-emitting plasma (e.g., NGC 1266; Alatalo et al. 2015), but disentangling the relative contributions of thermal and power-law emission would be difficult, without making further assumptions to reduce some of the free parameters of the combined model, given the limited constraints of the observations.

SPOG253, SPOG462, SPOG470, and SPOG224 all seem to have similar observed properties, namely X-ray emission dominated by thermal emission at temperatures around 0.5–0.7 keV, with luminosities generally of a similar order of magnitude ($L_X \sim 10^{40}$ erg s⁻¹), although SPOG470 looks to be a bit brighter. The relatively common presence of thermal emission in this sample suggests that either multiphase outflows or shocked X-ray emitting plasma, potentially due to interactions between AGN jets and the ISM (e.g., Ogle et al.

2014; Lanz et al. 2015; Appleton et al. 2018), may also be frequent in SPOGs.

Since thermal emission can also be associated with X-ray binaries and star formation, we tested the likelihood of this possibility by calculating the expected X-ray luminosity under the assumption that all of the H α emission in the Sloan Digital Sky Survey fiber¹⁹ was due to star formation. We calculated the associated star formation rate with the Kennicutt et al. (1994) relation and the associated X-ray binary luminosity using Equation (22) from Mineo et al. (2012). For all four of the galaxies where thermal models appear to be preferred, the X-ray binary luminosity is at least an order of magnitude less than the most likely X-ray luminosity from the forward modeling, indicating that the X-ray emission is unlikely to be solely due to X-ray binaries.

However, additional multiwavelength observations and analyses would be needed to confirm this interpretation and rule out nuclear starbursts as an alternative source. One possible avenue would be to use MIR spectra to search for warm molecular hydrogen emission lines indicative of shocked ISM. If these galaxies also have deeply buried AGNs responsible for outflows, like NGC 1266, or other AGN-driven shocks, then at least 75% of the sample would contain AGNs of modest to moderate luminosity and therefore accretion rate.

¹⁹ Data Release 7 spectra were taken through 3'' apertures, slightly larger than our X-ray extraction aperture.

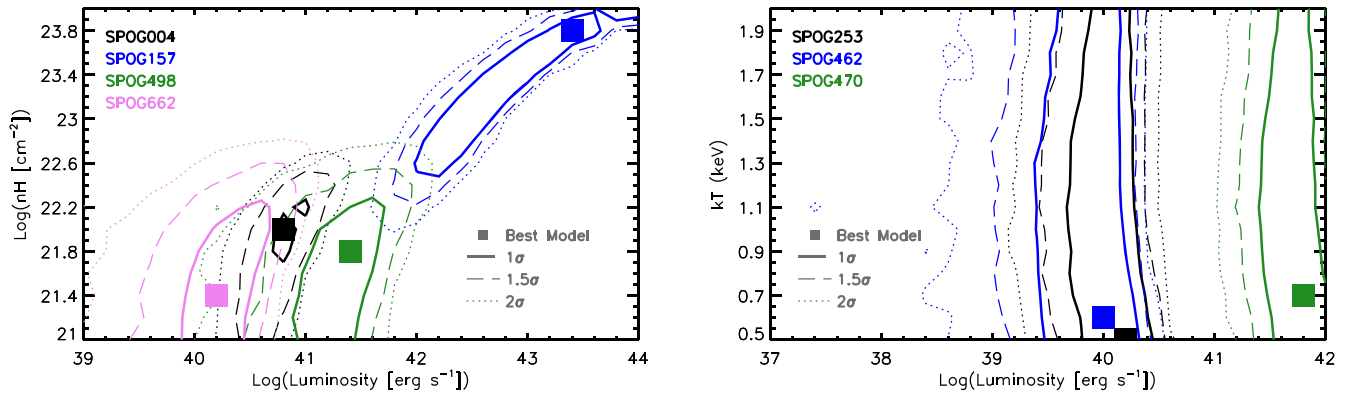


Figure 6. A comparison of the parameter spaces for the best models for our seven galaxies with significant detections. On the left, we show the four models that are significantly better matched with a power-law model. On the right, we show the three models that are better matched with a thermal model. The filled squares show the models with the highest fraction of mock spectra consistent with the observational constraints. The solid, dashed, and dotted lines show the range in which at least 68.3%, 86.6%, and 95.4% (corresponding to 1σ , 1.5σ , and 2σ of the mean of a normal distribution) of the mock spectra are consistent with the observation. The models outside each of these contours are rejected at the corresponding level.

While these AGNs are not radiatively powerful, this frequency of X-ray activity is high compared to the extragalactic populations in X-ray surveys. For field galaxies, as these SPOGs generally appear to be, Haggard et al. (2010) found that approximately 1% at redshifts $0.05 < z < 0.31$ had AGNs with $L_X \geq 10^{42}$ erg s $^{-1}$. Only SPOG157 meets this luminosity threshold, so the small-number statistics make it difficult to tell whether bright AGN activity is overrepresented in SPOGs at 8% (one of 12). However, low-luminosity AGN activity does seem to be higher than is found in other extragalactic populations. Young et al. (2012) investigated the presence of low-luminosity AGNs via variability in the 92 galaxies ($0.08 < z < 1.02$) in the 4 Ms Chandra Deep Field South (CDF-S) that do not contain AGNs with $L_X > 3 \times 10^{42}$ erg s $^{-1}$. They found that at least 20 ($\geq 22\%$) showed evidence of accretion onto a supermassive black hole, indicating that growth in these quiescent or low-luminosity phases could contribute significantly to black hole mass.

By comparison, the 50%–75% of our SPOGs showing at least low-luminosity AGN emission are suggestively higher.²⁰ This is consistent with the previous results, such as those of De Propriis & Melnick (2014), in finding that X-ray emission is common, but indicative of low-luminosity AGN activity rather than radiatively powerful AGNs. Further observations will be required, however, to better constrain the black hole and galactic bulge masses to see if growth was potentially needed at this transitional stage to bring the galaxies in agreement with the M – σ relation (e.g., McConnell & Ma 2013).

5.2. Implications for Timing of AGN Activity

The canonical picture of galaxy evolution via major mergers (e.g., Sanders et al. 1988; Hopkins et al. 2006) places AGN feedback prior to a post-starburst phase, requiring strong radiation from the AGN to drive out star-forming fuel. While this pathway may work well for some galaxies, others are likely to require different relative timings for these processes. For example, a significant fraction of two post-starburst samples showed significant remaining reservoirs of molecular gas (Rowlands et al. 2015; Alatalo et al. 2016b; French et al.

2018), and Schawinski et al. (2009) found similar reservoirs powering residual star formation in a sample of early-type galaxies. The galaxies in these samples require a mechanism to either complete the removal of this gas or otherwise suppress its ability to form stars. Schawinski et al. (2009) specifically concluded that low-luminosity AGN episodes were the most likely method by which this would be accomplished in their sources.

A delay between the starburst phase and the onset of AGN activity would be in line with a number of other studies. Wild et al. (2007, 2010) and Davies et al. (2007) found such delays in samples of low-redshift AGNs, many of which also had post-starburst signatures. Yesuf et al. (2014) and Pawlik et al. (2018) probed this question, starting with post-starburst galaxies, and found AGN signatures in a significant fraction. However, both studies also concluded that while AGNs may prevent the reemergence of star formation activity or help to finish quenching, the later onset indicated that it was unlikely that the AGN had precipitated the primary decrease in star formation activity.

This pathway with delayed AGN activity would explain our particular galaxies better than the canonical picture. While an earlier phase of luminous AGN activity may have taken place at the peak of any major merger that these galaxies may have experienced, the current AGN activity is much more consistent with lower luminosities, which can act to suppress residual star formation activity.

5.3. Effects of Sample Selection

In selecting the subset of SPOGs to observe with Chandra, we did not select our pilot sample to be representative of the full SPOG population. Instead, we focused on those with the most complete data sets. As such, our set of 12 had been detected in CO(1–0) (Alatalo et al. 2016b), with either IRAM or CARMA. The SPOGs selected for these submillimeter observations had in turn been required to be detected with WISE in the 22 μ m band (491/1067 SPOGs). While not all of the CO-observed SPOGs also had FIRST counterparts, we selected our Chandra targets from the subset that did.

This sample selection has several implications for the broader interpretation of what this sample can tell us about the population. First, the requirement of a CO detection means that these galaxies will still contain potential fuel for AGN

²⁰ Using Poisson statistics, the cumulative probability that at least six of the 12 in our sample would show low-luminosity AGN signatures were they to belong to the same population as the CDF-S set is 5.2%.

activity. Post-starburst galaxies have been shown to have molecular gas fractions that are more similar to star-forming galaxies than to the quiescent elliptical and lenticular galaxies that they are thought to be evolving into (French et al. 2015; Rowlands et al. 2015; Alatalo et al. 2016b). However, a mechanism such as a merger is likely necessary to disrupt the star-forming disk and help drive the gas toward the nucleus in order to feed the AGN (e.g., Hopkins 2012).

Second, the requirement of both a significant $22\ \mu\text{m}$ detection and a FIRST counterpart selected a pilot sample with preexisting indications of AGN activity. As such, these SPOGs may be some of those most likely to host an active AGN, and the AGN fraction in this sample may therefore be higher than in the overall SPOG population. However, IR, radio, and X-ray AGN selection criteria do not select the same AGNs (Hickox et al. 2009), suggesting that radio-bright AGNs may not necessarily be X-ray- or IR-bright. Indeed, Hickox et al. (2009) found that only $\sim 10\%$ of radio-selected AGNs were also selected in the IR, and, of those, only about half were also selected in X-rays. As such, it is possible that brighter X-ray AGNs exist within the set of SPOGs without FIRST counterparts. Extending the conclusions of this study to the larger post-starburst population, including E+A and K+A galaxies, is also complicated by the relatively younger age of SPOGs (see Figure 9 of Alatalo et al. 2016a) and the unclear timing of the AGN triggering during the transition to quiescence.

Third, the FIRST counterpart requirements may also indicate that, as radio AGNs, the feedback mode of the AGNs in these galaxies will tend to the mechanical rather than the radiative (e.g., Alexander & Hickox 2012). As such, the AGNs could still be important in helping the transition along. NGC 1266 shows that SPOGs can contain significant AGN-driven outflows (Alatalo et al. 2015). However, it also shows that, while such outflows can be effective at injecting turbulence into the ISM and pushing the gas outward from the nuclear region, these outflows are unlikely to fully eject the gas reservoirs out of the gravitational potential of these galaxies. Therefore, the AGNs in these systems may be better said to be helping maintain a lower level of star-forming activity, by reducing the amount of cold dense gas, rather than driving a permanent end to star formation, as would be the case with the removal of the remainder of the star-forming fuel. The significant fraction of the sample with X-ray emission consistent with thermal emission suggests that this may be a frequent process in these galaxies.

5.4. Future Work

Addressing the effects of sample selection in order to generalize these conclusions to the broader SPOG and post-starburst population will require larger samples of X-ray observations. As we have shown in this paper, the forward-modeling methodology allows us to place constraints even with minimal photons. The next step is clearly to apply this approach to all the observations of the post-starburst galaxies observed, primarily serendipitously, with Chandra, X-ray Multi-Mirror Mission (XMM)-Newton, Swift X-ray Telescope (Swift-XRT), NuSTAR, and eROSITA. The large sky coverage of eROSITA is particularly promising as a way of reducing the effects of selection biases, and extending to higher energies could give improved constraints on obscured systems, like SPOG157, and/or enable us to determine whether systems that

are thermally dominated at softer energies (e.g., SPOG253, NGC 1266) also have deeply buried AGNs.

A second area of improvement on which we are actively working is to determine how firm the forward-modeling constraints are. Our conclusions in this paper do not depend on the specific luminosity or obscuration of the model that matches best, but it would be useful to know how strong those constraints are and whether this approach tends to systematically over- or underestimate certain parameters. We are taking two approaches to testing this methodology. First, we will use new deeper XMM-Newton observations of SPOG157 (70 ks) and SPOG253 (63 ks). These should provide sufficient counts for spectral fitting, providing an independent constraint on the parameters of these two SPOGs to compare with the forward-modeling analysis. Further, as the two galaxies from this sample span the range of hardness ratios and model types, those analyses may also provide further guidance for the forward-modeling methodology. Second, we are applying the forward-modeling analysis to a set of Swift-Burst Alert Telescope (BAT) sources, whose parameters are well constrained by a combination of Swift-XRT and NuSTAR observations, to see how well the forward-modeling analysis recovers their luminosity and obscuration. That analysis will show the reliability of the forward-modeling constraints.

6. Summary

We performed a forward-modeling analysis for 12 post-starburst galaxies from the SPOG sample to constrain the parameters of their nuclear X-ray emission. At least seven of the 12 had significant X-ray detections in ~ 10 ks Chandra observations. However, none of these sources had more than 10 photons. We used the photon flux and the range of hardness ratios consistent with the observations to constrain the intrinsic 2–10 keV luminosity and obscuration column of a simple AGN model or the 0.5–8 keV luminosity and temperature of an APEC thermal model. For each galaxy, we tested 832 different models, for which we generated 1000 mock spectra each, to compare with the observed constraints.

Between 58% and 75% of the sample show evidence of AGN activity, depending on whether we include galaxies with weaker constraints, which could also be the result of thermal emission. The large majority of these are low-luminosity AGNs, and even the brightest, SPOG157, only has a luminosity of $\sim 3 \times 10^{43}\ \text{erg s}^{-1}$. Taken together, these analyses suggest that a large fraction of the supermassive black holes in SPOGs are active, especially compared to the broader population of field galaxies. However, they are clearly not sufficiently luminous to exert significant radiative feedback.

The selection criteria of this pilot sample may have selected both for and against X-ray-bright AGNs (see Section 5.3), so how well this conclusion can be extended to the larger SPOG sample and the broader post-starburst population remains unclear. The general SPOG selection tends to select galaxies with a younger stellar population, caught earlier in the transitional process, and its basis on line ratios rather than line strengths does not exclude as many galaxies that have line properties consistent with AGN or LINER emission. The resulting higher level of activity in these galaxies may reveal its importance to the initial phases of post-starburst transition, though it may not remain as prevalent throughout the post-starburst phase. FIRST detections of each of this sample's galaxies may also indicate that the mechanical mode of











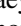
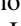
feedback is more common in this phase. Future analyses of existing and forthcoming X-ray data sets, as well as radio and IR signatures of AGNs, may provide greater clarity on the larger question of the timing and activity of AGNs in the full post-starburst phase.

L.L. thanks Alexander Nazarov for his contributions in helping to lay the groundwork for this analysis and Michael Ochs for useful discussions on Bayesian statistics. The scientific results reported in this article are based on observations made by the Chandra X-Ray Observatory. Support for this work was provided by the National Aeronautics and Space Administration through Chandra Award No. GO7-18093A issued by the Chandra X-Ray Observatory Center, which is operated by the Smithsonian Astrophysical Observatory for and on behalf of the National Aeronautics Space Administration (NASA), under contract NAS8-03060. L.L. and S.S. also acknowledge support from NASA through grant No. 80NSSC20K0050. Basic research in radio astronomy at the U.S. Naval Research Laboratory is supported by 6.1 Base Funding. A.M.M. acknowledges support from the National Science Foundation under grant No. 2009416.

Facility: CXO.

Software: Sherpa (Freeman et al. 2001; Doe et al. 2007).

ORCID iDs

Lauranne Lanz  <https://orcid.org/0000-0002-3249-8224>
 Sofia Stepanoff  <https://orcid.org/0000-0002-7850-7093>
 Ryan C. Hickox  <https://orcid.org/0000-0003-1468-9526>
 Katherine Alatalo  <https://orcid.org/0000-0002-4261-2326>
 Kate Rowlands  <https://orcid.org/0000-0001-7883-8434>
 Kristina Nyland  <https://orcid.org/0000-0003-1991-370X>
 Philip N. Appleton  <https://orcid.org/0000-0002-7607-8766>
 Mark Lacy  <https://orcid.org/0000-0002-3032-1783>
 Anne Medling  <https://orcid.org/0000-0001-7421-2944>
 John S. Mulchaey  <https://orcid.org/0000-0003-2083-5569>
 Elizaveta Sazonova  <https://orcid.org/0000-0001-6245-5121>
 Claudia Megan Urry  <https://orcid.org/0000-0002-0745-9792>

References

- Alatalo, K., Lacy, M., Lanz, L., et al. 2015, *ApJ*, 798, 31
 Alatalo, K., Cales, S. L., Rich, J. A., et al. 2016a, *ApJS*, 224, 38
 Alatalo, K., Lisenfeld, U., Lanz, L., et al. 2016b, *ApJ*, 827, 106
 Alatalo, K., Bitsakis, T., Lanz, L., et al. 2017, *ApJ*, 843, 9
 Alexander, D. M., & Hickox, R. C. 2012, *NewAR*, 56, 93
 Appleton, P. N., Diaz-Santos, T., Fadda, D., et al. 2018, *ApJ*, 869, 61
 Ardila, F., Alatalo, K., Lanz, L., et al. 2018, *ApJ*, 863, 28
 Baldry, I. K., Glazebrook, K., Brinkmann, J., et al. 2004, *ApJ*, 600, 681
 Baldwin, J. A., Phillips, M. M., & Terlevich, R. 1981, *PASP*, 93, 5
 Baloković, M., Brightman, M., Harrison, F. A., et al. 2018, *ApJ*, 854, 42
 Becker, R. H., White, R. L., & Helfand, D. J. 1995, *ApJ*, 450, 559
 Bell, E. F., McIntosh, D. H., Katz, N., & Weinberg, M. D. 2003, *ApJS*, 149, 289
 Brown, M. J. I., Moustakas, J., Caldwell, N., et al. 2009, *ApJ*, 703, 150
 Cicone, C., Maiolino, R., Sturm, E., et al. 2014, *A&A*, 562, A21
 Dadina, M. 2008, *A&A*, 485, 417
 Davies, R. I., Müller Sánchez, F., Genzel, R., et al. 2007, *ApJ*, 671, 1388
 De Propriis, R., & Melnick, J. 2014, *MNRAS*, 439, 2837
 Doe, S., Nguyen, D., Stawarz, C., et al. 2007, in ASP Conf. Ser. 376, *Astronomical Data Analysis Software and Systems XVI*, ed. R. A. Shaw, F. Hill, & D. J. Bell (San Francisco, CA: ASP), 543
 Freeman, P., Doe, S., & Siemiginowska, A. 2001, *Proc. SPIE*, 4477, 76
 French, K. D., Yang, Y., Zabludoff, A., et al. 2015, *ApJ*, 801, 1
 French, K. D., Yang, Y., Zabludoff, A. I., & Tremonti, C. A. 2018, *ApJ*, 862, 2
 Gehrels, N. 1986, *ApJ*, 303, 336
 Georgakakis, A., Nandra, K., Yan, R., et al. 2008, *MNRAS*, 385, 2049
 Goto, T. 2005, *MNRAS*, 357, 937
 Goto, T. 2007, *MNRAS*, 381, 187
 Haggard, D., Green, P. J., Anderson, S. F., et al. 2010, *ApJ*, 723, 1447
 HI4PI Collaboration, Ben Bekhti, N., Flöer, L., et al. 2016, *A&A*, 594, A116
 Hickox, R. C., Jones, C., Forman, W. R., et al. 2009, *ApJ*, 696, 891
 Hinshaw, G., Larson, D., Komatsu, E., et al. 2013, *ApJS*, 208, 19
 Hopkins, P. F. 2012, *MNRAS*, 420, L8
 Hopkins, P. F., Hernquist, L., Cox, T. J., et al. 2006, *ApJS*, 163, 1
 Hopkins, P. F., Hernquist, L., Cox, T. J., & Kereš, D. 2008, *ApJS*, 175, 356
 Hopkins, P. F., & Quataert, E. 2010, *MNRAS*, 407, 1529
 Kauffmann, G., Heckman, T. M., White, S. D. M., et al. 2003, *MNRAS*, 341, 54
 Kennicutt, R. C. J. 1998, *ApJ*, 498, 541
 Kennicutt, R. C. J., Tamblyn, P., & Congdon, C. E. 1994, *ApJ*, 435, 22
 Kewley, L. J., Groves, B., Kauffmann, G., & Heckman, T. 2006, *MNRAS*, 372, 961
 Lanz, L., Ogle, P. M., Alatalo, K., & Appleton, P. N. 2016, *ApJ*, 826, 29
 Lanz, L., Ogle, P. M., Evans, D., et al. 2015, *ApJ*, 801, 17
 Lotz, M., Dolag, K., Remus, R.-S., & Burkert, A. 2021, *MNRAS*, 506, 4516
 Maiolino, R., & Risaliti, G. 2007, in ASP Conf. Ser. 373, *The Central Engine of Active Galactic Nuclei*, ed. L. C. Ho & J. W. Wang (San Francisco, CA: ASP), 447
 McConnell, N. J., & Ma, C.-P. 2013, *ApJ*, 764, 184
 Melnick, J., & De Propriis, R. 2013, *MNRAS*, 431, 2034
 Meusinger, H., Brünecke, J., & Schalldachs, P. 2017, *A&A*, 597, A134
 Mineo, S., Gilfanov, M., & Sunyaev, R. 2012, *MNRAS*, 419, 2095
 Nielsen, D. M., Ridgway, S. E., De Propriis, R., & Goto, T. 2012, *ApJL*, 761, L16
 Noeske, K. G., Weiner, B. J., Faber, S. M., et al. 2007, *ApJL*, 660, L43
 Ogle, P. M., Lanz, L., & Appleton, P. N. 2014, *ApJL*, 788, L33
 Park, T., Kashyap, V. L., Siemiginowska, A., et al. 2006, *ApJ*, 652, 610
 Pawlik, M. M., Wild, V., Walcher, C. J., et al. 2016, *MNRAS*, 456, 3032
 Pawlik, M. M., Taj Aldeen, L., Wild, V., et al. 2018, *MNRAS*, 477, 1708
 Piconcelli, E., Jimenez-Bailón, E., Guainazzi, M., et al. 2005, *A&A*, 432, 15
 Quintero, A. D., Hogg, D. W., Blanton, M. R., et al. 2004, *ApJ*, 602, 190
 Rowlands, K., Wild, V., Nesvadba, N., et al. 2015, *MNRAS*, 448, 258
 Sanders, D. B., Soifer, B. T., Elias, J. H., et al. 1988, *ApJ*, 325, 74
 Sazonova, E., Alatalo, K., Rowlands, K., et al. 2021, *ApJ*, 919, 134
 Schawinski, K., Lintott, C. J., Thomas, D., et al. 2009, *ApJ*, 690, 1672
 Schawinski, K., Urry, C. M., Simmons, B. D., et al. 2014, *MNRAS*, 440, 889
 Shin, M.-S., Strauss, M. A., & Tojeiro, R. 2011, *MNRAS*, 410, 1583
 Smercina, A., Smith, J. D. T., Dale, D. A., et al. 2018, *ApJ*, 855, 51
 Smith, R. K., Brickhouse, N. S., Liedahl, D. A., & Raymond, J. C. 2001, *ApJL*, 556, L91
 Somerville, R. S., Hopkins, P. F., Cox, T. J., Robertson, B. E., & Hernquist, L. 2008, *MNRAS*, 391, 481
 Springel, V., Di Matteo, T., & Hernquist, L. 2005a, *MNRAS*, 361, 776
 Springel, V., Di Matteo, T., & Hernquist, L. 2005b, *ApJL*, 620, L79
 Stern, D., Assef, R. J., Benford, D. J., et al. 2012, *ApJ*, 753, 30
 Strateva, I., Ivezić, Ž., Knapp, G. R., et al. 2001, *AJ*, 122, 1861
 Sturm, E., González-Alfonso, E., Veilleux, S., et al. 2011, *ApJL*, 733, L16
 Toomre, A., & Toomre, J. 1972, *ApJ*, 178, 623
 Veilleux, S., & Osterbrock, D. E. 1987, *ApJS*, 63, 295
 Weisskopf, M. C., Tananbaum, H. D., Van Speybroeck, L. P., & O'Dell, S. L. 2000, *Proc. SPIE*, 4012, 2
 Wild, V., Heckman, T., & Charlot, S. 2010, *MNRAS*, 405, 933
 Wild, V., Kauffmann, G., Heckman, T., et al. 2007, *MNRAS*, 381, 543
 Williams, D. R. A., Pahari, M., Baldi, R. D., et al. 2022, *MNRAS*, 510, 4909
 Yang, Y., Zabludoff, A. I., Zaritsky, D., & Mihos, J. C. 2008, *ApJ*, 688, 945
 Yusef, H. M., Faber, S. M., Trump, J. R., et al. 2014, *ApJ*, 792, 84
 Young, M., Brandt, W. N., Xue, Y. Q., et al. 2012, *ApJ*, 748, 124
 Zabludoff, A. I., Zaritsky, D., Lin, H., et al. 1996, *ApJ*, 466, 104
 Zheng, Y., Wild, V., Lahén, N., et al. 2020, *MNRAS*, 498, 1259